


Article

Calibration of Luminosity Correlations of Gamma-Ray Bursts Using Quasars

Sarveshkumar Purohit¹ and Shantanu Desai^{2,*} 

¹ Department of Artificial Intelligence, Indian Institute of Technology, Hyderabad 502284, Telangana, India; sarveshpurohit84@gmail.com or ai22mtech14006@iith.ac.in

² Department of Physics, Indian Institute of Technology, Hyderabad 502284, Telangana, India

* Correspondence: shntn05@gmail.com

Abstract: In order to test the efficacy of gamma-ray bursts (GRBs) as cosmological probes, we characterize the scatter in the correlations between six pairs of GRB observables. However, some of these observables depend on the luminosity distance, for which one needs to assume an underlying cosmological model. In order to circumvent this circularity problem, we use X-ray and UV fluxes of quasars as distance anchors to calculate the luminosity distance in a model-independent manner, which, in turn, is used to calculate the GRB-related quantities. We find that all six pairs of regression relations show high intrinsic scatter for both low- and high-redshift samples. This implies that these GRB observables cannot be used as model-independent high-precision cosmological probes.

Keywords: gamma-ray bursts; quasars; regression

1. Introduction

Gamma-ray bursts (GRBs) are single-shot explosions located at cosmological distances, which were first detected in the 1960s and have been observed across ten decades at energies from the keV to the over 10 TeV range [1,2]. They are located at cosmological distances, although a distinct time dilation signature in the light curves is yet to be demonstrated [3–5]. Because of their high energies and cosmological distances, they have also proven to be very good probes of fundamental physics, such as for testing Lorentz invariance violations and quantum gravity [6–10]. GRBs are traditionally divided into two categories based on their durations, with long and short GRBs lasting more than and less than two seconds, respectively [11]. Long GRBs are usually associated with core-collapse supernovae [12] and short GRBs with neutron star mergers [13]. There are, however, many exceptions to this conventional dichotomy [14–17], and many claims of additional GRB sub-classes have also been discussed in literature [18–21].

GRBs have been proposed as distance indicators or standard candles for cosmological purposes over the past two decades due to putative correlations between myriad GRB observables in both the prompt and afterglow emission phases [22–27]. These correlations have often been used to estimate cosmological parameters [28]. An up-to-date review of all GRB correlations in the prompt and afterglow phases, along with the cosmological applications of these relations, can be found in [29].

However, there is an inherent circularity problem in using GRB observables as cosmological probes since the calculation of these observables is based on an underlying cosmological model. However, in any case, the correlations should be preserved. To evade this circularity problem, two methodologies have been used in the literature. One way is to simultaneously constrain the GRB correlations and the cosmological parameters [30,31]. Alternatively, a large number of ancillary probes have also been used to obtain cosmology-independent estimates of distances corresponding to GRB redshifts, such as Type Ia SNs, cosmic chronometers, BAO $H(z)$ measurements, the X-ray and UV luminosities of quasars, galaxy clusters, etc. [32] (and the references therein).



Citation: Purohit, S.; Desai, S. Calibration of Luminosity Correlations of Gamma-Ray Bursts Using Quasars. *Galaxies* **2024**, *12*, 69. <https://doi.org/10.3390/galaxies12060069>

Academic Editors: Maria Giovanna Dainotti and Nissim Fraija

Received: 10 August 2024

Revised: 3 September 2024

Accepted: 20 October 2024

Published: 25 October 2024



Copyright: © 2024 by the authors. Licensee MDPI, Basel, Switzerland. This article is an open access article distributed under the terms and conditions of the Creative Commons Attribution (CC BY) license (<https://creativecommons.org/licenses/by/4.0/>).

Here, we focus on the correlations between six pairs of GRB observables— $\tau_{lag} - L$, $V - L$, $E_p - L$, $E_p - E_\gamma$, $\tau_{RT} - L$, $E_p - E_{iso}$ —that were proposed in [33] (see also [34]).¹ The aforementioned work simultaneously fitted for the cosmology and the regression relations between the above parameters [33]. Subsequently, these correlations were then studied by obtaining model-independent distances to the GRBs using the Pantheon compilation [39] of Type Ia SNe in [40] (referred to as T21 hereafter). Here, we carry out a variant of the analysis conducted in T21 by using the X-ray and UV luminosities of quasars instead of Type Ia SNe to probe the same correlations first considered in [33]. We note that quasars were used previously to probe the efficacy of the Amati relation [41] for the GRB datasets in [30,42,43].

The outline of this manuscript is as follows. We discuss the datasets used in this work in Section 2. Our analysis and results can be found in Section 3. We conclude in Section 4.

2. Datasets

We used the same GRB datasets as those considered in T21, which were originally obtained from [33]. This work considered a sample of 116 long GRBs with redshifts between 0.17 and 8.2. This sample consisted of GRBs observed by SWIFT until 2012 in conjunction with 69 additional GRBs from other detectors obtained before the launch of the SWIFT satellite [38]. The dataset in [38] consisted of long GRBs with well-measured and robust redshifts. For the additional SWIFT GRBs considered in [33], any long GRB with more than 100% error for any observable was discarded. The observables assembled for each GRB consist of the bolometric peak flux (P_{bolo}), the bolometric fluence (S_{bolo}), the beaming factor (F_{beam}), the time lag between low- and high-energy photon light curves (τ_{lag}), the peak energy of the spectrum (E_p), the minimum rise time of the peaks for which the light curve rises by half its peak flux (τ_{RT}), and the variability in the light curve (V), along with their 1σ error bars. Among these measurements, τ_{RT} , E_p , τ_{lag} , and V were obtained directly from spectral analysis, whereas P_{bolo} and S_{bolo} could be obtained from the GRB spectrum observed, as outlined in [33]. In a future work, we shall update this dataset using the entire SWIFT catalog. In order to test for potential correlations, one needs to calculate the isotropic peak luminosity (L), the isotropic equivalent energy (E_{iso}), and the collimation-corrected energy (E_γ), which, in turn, depend on the luminosity distance (D_L), for which one needs to posit an underlying cosmological model. The relation between L and P_{bolo} is given by

$$L = 4\pi D_L^2 P_{bolo}, \quad (1)$$

E_{iso} is related to D_L using

$$E_{iso} = 4\pi D_L^2 S_{bolo} (1+z)^{-1} \quad (2)$$

Finally E_γ is given by

$$E_\gamma = 4\pi D_L^2 S_{bolo} F_{beam} (1+z)^{-1}, \quad (3)$$

where F_{beam} is the beaming factor, which was estimated using the empirical formula derived in [44].

This dataset was used to study six different pairs of luminosity correlations, $\tau_{lag} - L$, $V - L$, $E_p - L$, $E_p - E_\gamma$, $\tau_{RT} - L$, and $E_p - E_{iso}$, where some of the above variables were scaled according to redshift, as explained in the next section. To circumvent this circularity problem, a combined fit to linear regression between the above variables and the underlying cosmology model was made [33]. The intrinsic scatter of the $V - L$ correlation was found to be very large, but the other variables had a tight correlation with a negligible redshift evolution. This same set of correlations was considered before in T21 using a model-agnostic approach without assuming an underlying cosmological model. For this purpose, a model-independent estimate of D_L at each GRB redshift was obtained using deep learning and Gaussian-process-based regression using Type Ia supernova data, which overlap in their redshifts with those of the GRBs. T21 also tested for a redshift evolution for the same six regression relations (considered in [33]) by dividing the GRB dataset into low-redshift

and high-redshift samples. Among these, only $E_p - E_\gamma$ was found to have no redshift evolution [40].

The Quasar Dataset

In order to calculate D_L corresponding to a given GRB redshift, instead of Type Ia SNs, we use quasars as the distance anchors. Quasars consist of active galactic nuclei, where the energy release occurs due to the accretion onto a supermassive black hole. Quasars have been detected up to a redshift of $z = 7$ and therefore span the same redshift range as GRBs. Quasars have been observed throughout the electromagnetic spectrum [45]. A tight scaling relation between the optical–UV flux at a rest frame wavelength of 2500 Å and the X-ray flux at a rest frame energy of 2 keV of a quasar has been asserted, which is independent of redshift [46].

The value of D_L at a given redshift is obtained from a quasar’s X-ray and UV flux as follows [46,47]:

$$\log D_L = \frac{[\log F_X - \beta - \gamma(\log F_{UV} + 27.5)]}{2(\gamma - 1)} - 0.5 \log(4\pi) + 28.5, \quad (4)$$

where F_X and F_{UV} are the flux densities (in erg/s/cm²/Hz) $\beta \approx 8.2$ and $\gamma = 0.6$. This relation was obtained assuming a Hubble constant value of $H_0 = 70$ km/sec/Mpc. Lusso et al. [47] constructed a clean sample of 2,421 optically selected quasars spanning a redshift range of $0.006 \leq z \leq 7.52$ (with a dispersion in the $L_X - L_{UV}$ relation of 0.24 dex), where the distance modulus (μ) and the associated errors were obtained using D_L from the above equation as below:

$$\mu = 5 \log(D_L) - 5 \log(10 \text{pc}) \quad (5)$$

Therefore, one can obtain the distance modulus for each quasar’s redshift from the quasar’s X-ray and UV fluxes. We note, however, that concerns have been raised that this quasar dataset [47] may be not be standardizable [48–50], which is probably caused by the dust extinction in the $L_X - L_{UV}$ relation [51]. Nevertheless, since the quasar dataset in [47] has been used to test for GRB correlations [41], we use this QSO dataset to derive distance anchors for direct comparison with the scatter obtained in T21 using Type Ia supernovae. More detailed studies using a pure quasar sample will be deferred to a future work.

3. Analysis and Results

The first step in the analysis involves obtaining a model-independent estimate of D_L from the quasar dataset. As mentioned in the previous section, we start with the μ and z values for 2421 quasars. With these data, we carry out a non-parametric reconstruction of μ at any redshift z using Gaussian process regression (GPR). GPR is a generalization of a Gaussian distribution, characterized by a mean and a covariance function (usually called the kernel function) [52]. For the GPR implementation, we use the publicly available Python package `sklearn` [53] to reconstruct the distance modulus (μ) as a function of the redshift (z) as follows: The kernel we have used for the regression is a sum of linear and constant kernels. A linear kernel with an exponent captures the relations in the data, and a constant kernel is used to scale the magnitude. The GPR reconstruction of μ along with the associated 1σ error bars can be found in Figure 1. Once we have reconstructed μ at any value of z , we can estimate D_L by inverting Equation (5). The errors in D_L can be obtained using standard error propagation. We then obtain L and E_{iso} using Equation (1) and Equation (2), respectively.

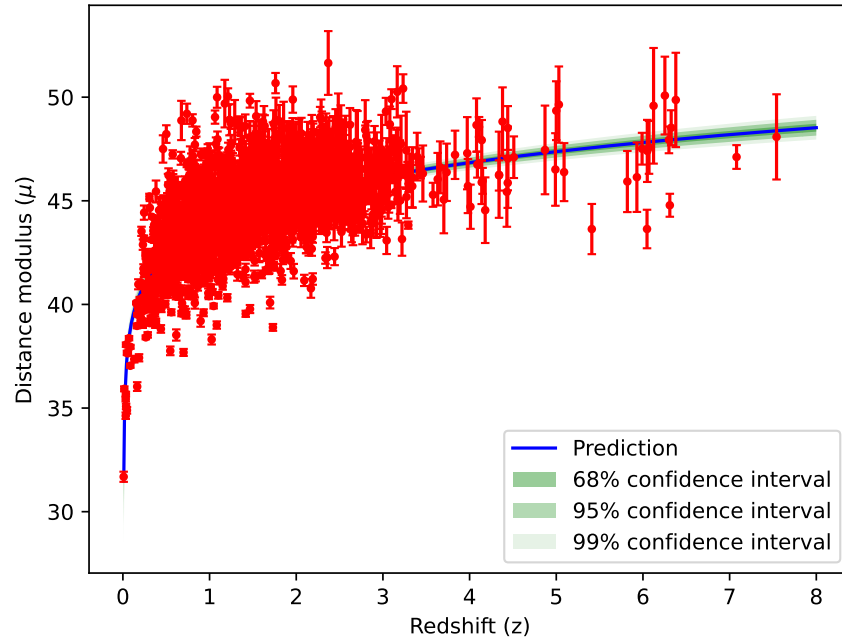


Figure 1. Reconstruction of μ with GPR using X-ray and UV fluxes for 2421 quasars.

We then carry out linear regression between the six aforementioned GRB quantities in log space as follows:

$$\log \frac{L}{\text{erg s}^{-1}} = a_1 + b_1 \log \frac{\tau_{\text{lag},i}}{0.1 \text{ s}}, \quad (6)$$

$$\log \frac{L}{\text{erg s}^{-1}} = a_2 + b_2 \log \frac{V_i}{0.02}, \quad (7)$$

$$\log \frac{L}{\text{erg s}^{-1}} = a_3 + b_3 \log \frac{E_{p,i}}{300 \text{ keV}} \quad (8)$$

$$\log \frac{E_\gamma}{\text{erg}} = a_4 + b_4 \log \frac{E_{p,i}}{300 \text{ keV}}, \quad (9)$$

$$\log \frac{L}{\text{erg s}} = a_5 + b_5 \log \frac{\tau_{\text{RT},i}}{0.1 \text{ s}}, \quad (10)$$

$$\log \frac{E_{\text{iso}}}{\text{erg}} = a_6 + b_6 \log \frac{E_{p,i}}{300 \text{ keV}} \quad (11)$$

where $\tau_{\text{RT},i} = \tau_{\text{RT}}/(1+z)$, $\tau_{\text{lag},i} = \tau_{\text{lag}}/(1+z)$, $V_i = V(1+z)$, and $E_{p,i} = E_p(1+z)$.

To obtain the best-fit parameters for each of the above equations, we apply D'Agostini's likelihood, which incorporates errors into both the ordinate and abscissa [54]:

$$\mathcal{L}(\sigma_{\text{int}}, a, b) \propto \prod_i \frac{1}{\sqrt{\sigma_{\text{int}}^2 + \sigma_{y_i}^2 + b^2 \sigma_{x_i}^2}} \times \exp \left[-\frac{(y_i - a - bx_i)^2}{2(\sigma_{\text{int}}^2 + \sigma_{y_i}^2 + b^2 \sigma_{x_i}^2)} \right], \quad (12)$$

where x and y denote the abscissa and the ordinate, and σ_{x_i} and σ_{y_i} are the corresponding errors; σ_{int} denotes the intrinsic scatter in each regression relation. To obtain the best-fit values for each of the parameters, we apply Bayesian regression and sample the posterior using the emcee MCMC sampler [55]. We use uniform priors on both a and b . Since we have obtained d_L using quasar UV and X-ray fluxes without an underlying cosmological model, we do not need to impose any priors onto the cosmological parameters.

In order to study the evolution of the aforementioned correlations with redshift, we bifurcate the GRB dataset into two subsamples corresponding to the same redshift intervals as T21: the low- z sample ($z \leq 1.4$) which consists of 50 GRBs, and the high- z sample ($z > 1.4$), which consists of 66 GRBs. We investigate the redshift dependence of the luminosity correlations for these two subsamples. We also show the results for the full GRB sample.

The best-fit intervals at 68%, 90%, and 99% credible intervals for all six regression relations can be found in Figure 2 for the full GRB sample and also after splitting the sample based on redshift. The scatter plots between the six pairs of variables along with the best fits are shown in Figure 3. We find that our results for the slope, intercept, and intrinsic scatter for almost all six scaling relations are consistent with those obtained in T21. The only exception is the $E_p - E_\gamma$ or Amati correlation, where we see an intrinsic scatter of 26–40%, whereas the intrinsic scatter was found to be $< 23\%$ in T21. We find that the values for the slope and the intercept are consistent or at most $1 - 2\sigma$ discrepant between the low-redshift and high-redshift samples, indicating negligible evolution of the scaling relations. Furthermore, all six regression relations show a high intrinsic scatter of greater than 30%. This includes the Amati relation, where we see a large scatter of 47% when we consider the full data sample, similar to our results of using galaxy clusters as the distance anchors [32]. Therefore, the regression relations between these observables using the quasar dataset in [47] as the distance anchors, which have large dispersion, cannot be used as model-independent probes of cosmological parameters. Another possible reason for this is the GRB dataset we have analyzed is not standardizable, and one needs to check for this before trying to calibrate it [48–50].

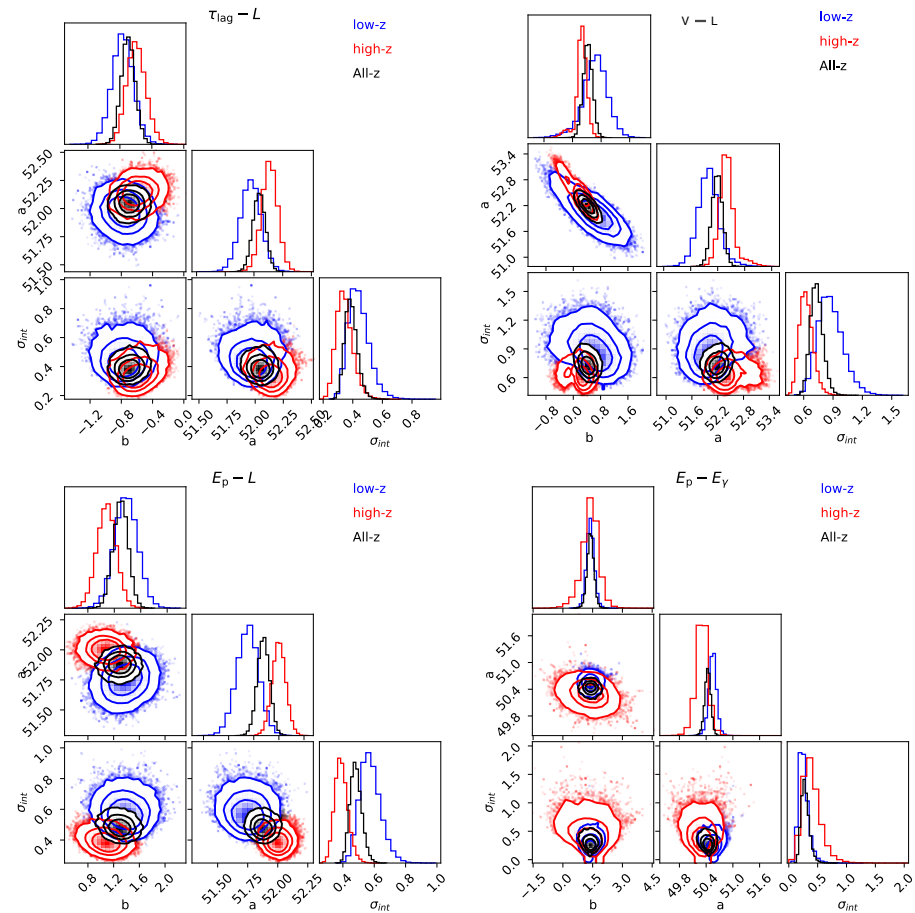


Figure 2. Cont.

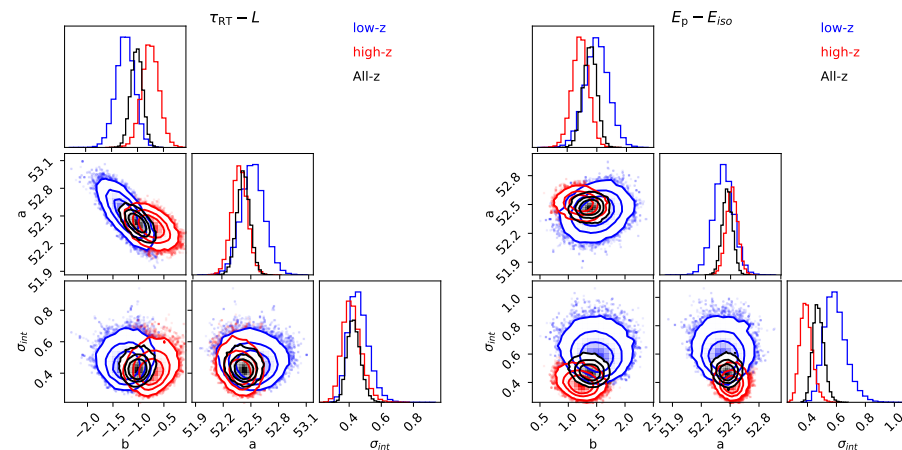


Figure 2. The 68%,90%, and 99% credible intervals along with the marginalized PDFs for the parameters for the regression relations between six pairs of GRB observables for low-redshift ($z < 1.4$) and high-redshift ($z > 1.4$) samples, as well as the full GRB dataset.

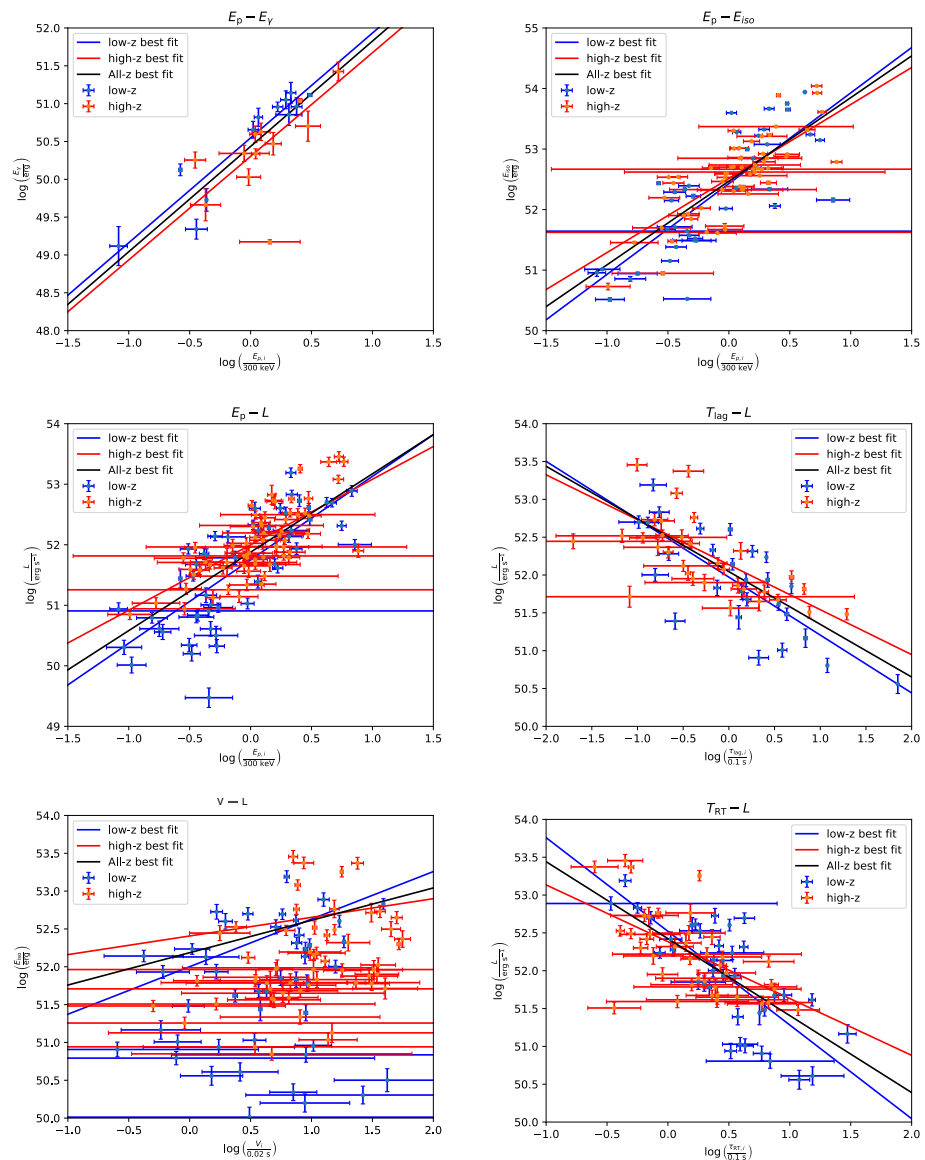


Figure 3. The luminosity correlations for low- z and high- z GRBs. The error bars denote the 1σ uncertainties. The lines depict the best-fit results.

4. Conclusions

The recent work T21 studied the empirical correlations among six pairs of GRB observables for 116 long GRBs (first considered in [33]) in order to test their efficacy as cosmological probes. However, one needs an estimate of the luminosity distance, which depends on an underlying cosmological model, to calculate some of these GRB observables. In order to avoid this circularity problem, luminosity distances from Type Ia supernovae were used as distance anchors, and the corresponding distance at a given GRB redshift was obtained using Artificial Neural Network-based regression.

In this work, we carried out the same exercise as in T21 but used the X-ray and UV fluxes of quasars instead of Type Ia supernovae in order to obtain the luminosity distance at a given GRB redshift. Interpolation was applied using Gaussian process regression. Similar to T21, we tested the correlations for both low-redshift and high-redshift samples after bifurcating the dataset at $z = 1.4$. Our results for the best-fit values for all the six regression relations can be found in Table 1. The marginalized credible intervals are shown in Figure 2, whereas the scatter plots for the six regression relations are shown in Figure 3. Our conclusions are as follows:

- The slopes and intercepts agree with the corresponding results from T21 for both low and high redshift, as well as the full sample.
- Our intrinsic scatter for almost all the scaling relations is comparable to that found in T21. The only exception is the Amati relation, where we see a much higher intrinsic scatter compared to in T21.
- Although there is negligible redshift evolution in the scaling relations, the high intrinsic scatter implies that we cannot use these GRB observables for model-independent estimates of cosmological parameters.
- We should note that another possible reason for the large scatter could be that the quasar dataset in [47] cannot be used to obtain distance anchors [48–50] or that the GRB dataset is not standardizable. One possibility would be to use the quasar reverberation-mapped observations discussed in [56] as distance anchors up to a redshift of $z = 3.4$.

In the spirit of open science, we have made all of our analysis code and data publicly available at <https://github.com/saarvesh/MTechThesis/tree/main/Final> as of 22 October 2024. In a future work, we shall also update the analysis using the latest SWIFT data.

Table 1. The best-fit parameters for GRB luminosity correlations. N is the number of GRBs in each subsample.

Correlation	Sample	N	a	b	σ_{int}
$\tau_{\text{lag}} - L$	low-z	37	51.97 ± 0.09	-0.77 ± 0.14	0.44 ± 0.07
	high-z	32	52.14 ± 0.07	-0.59 ± 0.12	0.35 ± 0.06
	all z	69	52.04 ± 0.06	-0.69 ± 0.09	0.39 ± 0.04
$V - L$	low-z	47	52.00 ± 0.24	0.63 ± 0.36	0.88 ± 0.13
	high-z	57	52.41 ± 0.18	0.25 ± 0.17	0.63 ± 0.07
	all z	104	52.19 ± 0.12	0.43 ± 0.13	0.73 ± 0.06
$E_p - L$	low-z	50	51.75 ± 0.09	1.38 ± 0.18	0.58 ± 0.07
	high-z	66	51.99 ± 0.06	1.08 ± 0.15	0.39 ± 0.04
	all z	116	51.88 ± 0.05	1.29 ± 0.11	0.48 ± 0.04
$E_p - E_\gamma$	low-z	12	50.55 ± 0.09	1.39 ± 0.20	0.26 ± 0.09
	high-z	12	50.30 ± 0.14	1.37 ± 0.44	0.39 ± 0.16
	all z	24	50.43 ± 0.07	1.39 ± 0.17	0.29 ± 0.07
$\tau_{\text{RT}} - L$	low-z	39	52.52 ± 0.12	-1.24 ± 0.18	0.46 ± 0.06
	high-z	40	52.38 ± 0.08	-0.75 ± 0.17	0.42 ± 0.06
	all z	79	52.42 ± 0.07	-1.02 ± 0.11	0.43 ± 0.041
$E_p - E_{\text{iso}}$	low-z	40	52.43 ± 0.10	1.49 ± 0.20	0.59 ± 0.08
	high-z	61	52.51 ± 0.06	1.22 ± 0.14	0.39 ± 0.04
	all z	101	52.47 ± 0.05	1.38 ± 0.12	0.48 ± 0.04

Author Contributions: Both authors contributed to the formal analysis and writing. All authors have read and agreed to the published version of the manuscript.

Funding: This research received no external funding.

Data Availability Statement: Data has been obtained from external papers cited in the manuscript and can also be made available from a reasonable request to the authors.

Acknowledgments: This work builds upon the M.Tech thesis of Shreeprasad Bhat, and we are grateful to him for sharing his code. We are grateful to Bharat Ratra for comments on the manuscript. We also acknowledge the anonymous referees for their useful feedback on the manuscript.

Conflicts of Interest: The authors declare no conflicts of interest.

Note

- ¹ We note that among the above correlations, the $E_p - E_\gamma$ relation is often referred to as the Amati relation, such as in literature [35]. Also, the correlation between E_p and L is also known as the Yonetoku relation and has been widely studied in the literature [36,37]. All the other correlations were first considered in [38].

References

- Kumar, P.; Zhang, B. The Physics of Gamma-Ray Bursts and Relativistic Jets. *Phys. Rep.* **2015**, *561*, 1–109.
- Yu, Y.-W.; Gao, H.; Wang, F.-Y.; Zhang, B.-B. *Handbook of X-Ray and Gamma-Ray Astrophysics*; Bambi, C., Santangelo, A., Eds.; Springer: Berlin/Heidelberg, Germany, 2022; p. 31.
- Kocevski, D.; Petrosian, V. On the Lack of Time Dilation Signatures in Gamma-Ray Burst Light Curves. *Astrophys. J.* **2013**, *765*, 116. [[CrossRef](#)]
- Littlejohns, O.M.; Butler, N.R. Investigating signatures of cosmological time dilation in duration measures of prompt gamma-ray burst light curves. *Mon. Not. R. Astron. Soc.* **2014**, *444*, 3948–3960. [[CrossRef](#)]
- Singh, A.; Desai, S. Search for Cosmological time dilation from Gamma-Ray Bursts—A 2021 status update. *JCAP* **2022**, *2022*, 010. [[CrossRef](#)]
- Amelino-Camelia, G.; Ellis, J.; Mavromatos, N.E.; Nanopoulos, D.V.; Sarkar, S. Tests of quantum gravity from observations of γ -ray bursts. *Nature* **1998**, *393*, 763–765. [[CrossRef](#)]
- Abdo, A.A.; Ackermann, M.; Ajello, M.; Asano, K.; Atwood, W.B.; Axelsson, M.; Baldini, L.; Ballet, J.; Barbiellini, G.; Baring, M.G.; et al. A limit on the variation of the speed of light arising from quantum gravity effects. *Nature* **2009**, *462*, 331–334. [[CrossRef](#)]
- Vasileiou, V.; Jacholkowska, A.; Piron, F.; Bolmont, J.; Couturier, C.; Granot, J.; Stecker, F.W.; Cohen-Tanugi, J.; Longo, F. Constraints on Lorentz Invariance Violation from Fermi-Large Area Telescope Observations of Gamma-Ray Bursts. *Phys. Rev. D* **2013**, *87*, 122001. [[CrossRef](#)]
- Vasileiou, V.; Granot, J.; Piran, T.; Amelino-Camelia, G. A Planck-Scale Limit on Spacetime Fuzziness and Stochastic Lorentz Invariance Violation. *Nat. Phys.* **2015**, *11*, 344–346. [[CrossRef](#)]
- Desai, S. *Recent Progress on Gravity Tests. Challenges and Future Perspectives*; Bambi, C., Cárdenas-Avendaño, A., Eds.; Springer: Singapore, 2024; pp. 433–463.
- Kouveliotou, C.; Meegan, C.A.; Fishman, G.J.; Bhat, N.P.; Briggs, M.S.; Koshut, T.M.; Paciesas, W.S.; Pendleton, G.N. Identification of two classes of gamma-ray bursts. *Astrophys. J. Lett.* **1993**, *413*, L101–L104. [[CrossRef](#)]
- Woosley, S.E.; Bloom, J.S. The Supernova—Gamma-Ray Burst Connection. *Ann. Rev. Astron. Astrophys.* **2006**, *44*, 507–556. [[CrossRef](#)]
- Nakar, E. Short-Hard Gamma-Ray Bursts. *Phys. Rep.* **2007**, *442*, 166–236. [[CrossRef](#)]
- Gehrels, N.; Norris, J.P.; Barthelmy, S.D.; Granot, J.; Kaneko, Y.; Kouveliotou, C.; Markwardt, C.B.; Mészáros, P.; Nakar, E.; Nousek, J.A.; et al. A new γ -ray burst classification scheme from GRB 060614. *Nature* **2006**, *444*, 1044–1046. [[CrossRef](#)]
- Ahumada, T.; Singer, L.P.; Anand, S.; Coughlin, M.W.; Kasliwal, M.M.; Ryan, G.; Andreoni, I.; Cenko, S.B.; Fremming, C.; Kumar, H.; et al. Discovery and confirmation of the shortest gamma ray burst from a collapsar. *Nat. Astron.* **2021**, *5*, 917–927. [[CrossRef](#)]
- Troja, E.; Fryer, C.L.; O’Connor, B.; Ryan, G.; Dichiaro, S.; Kumar, A.; Ito, N.; Gupta, R.; Wollaeger, R.T.; Norris, J.P.; et al. A nearby long gamma-ray burst from a merger of compact objects. *Nature* **2022**, *612*, 228–231. [[CrossRef](#)]
- Yang, Y.-H.; Troja, E.; O’Connor, B.; Fryer, C.L.; Im, M.; Durbak, J.; Paek, G.S.H.; Ricci, R.; Bom, C.R.; Gillanders, J.H.; et al. A lanthanide-rich kilonova in the aftermath of a long gamma-ray burst. *Nature* **2024**, *626*, 742–745. [[CrossRef](#)]
- Norris, J.P.; Bonnell, J.T. Short Gamma-Ray Bursts with Extended Emission. *Astrophys. J.* **2006**, *643*, 266. [[CrossRef](#)]
- Kulkarni, S.; Desai, S. Classification of Gamma-Ray Burst durations using robust model-comparison techniques. *Astrophys. Space Sci.* **2017**, *362*, 70. [[CrossRef](#)]
- Tóth, B.G.; Rácz, I.I.; Horváth, I. Gaussian-mixture-model-based cluster analysis of gamma-ray bursts in the BATSE catalog. *Mon. Not. R. Astron. Soc.* **2019**, *486*, 4823–4828. [[CrossRef](#)]
- Bhave, A.; Kulkarni, S.; Desai, S.; Srijith, P.K. Two Dimensional Clustering of Gamma-Ray Bursts using durations and hardness. *Astrophys. Space Sci.* **2022**, *367*, 39. [[CrossRef](#)]

22. Dainotti, M.G.; Amati, L. Gamma-ray burst prompt correlations: Selection and instrumental effects. *PASP* **2018**, *130*, 051001. [[CrossRef](#)]
23. Parsotan, T.; Ito, H. GRB Prompt Emission: Observed Correlations and Their Interpretations. *Universe* **2022**, *8*, 310. [[CrossRef](#)]
24. Dainotti, M.G.; Vecchio, R.D. Gamma Ray Burst afterglow and prompt-afterglow relations: An overview. *New Astron. Rev.* **2017**, *77*, 23–61. [[CrossRef](#)]
25. Luongo, O.; Muccino, M. Intermediate redshift calibration of Gamma-ray Bursts and cosmic constraints in non-flat cosmology. *Mon. Not. R. Astron. Soc.* **2023**, *518*, 2247–2255. [[CrossRef](#)]
26. Dainotti, M.G.; Nielson, V.; Sarracino, G.; Rinaldi, E.; Nagataki, S.; Capozziello, S.; Gnedin, O.Y.; Bargiacchi, G. Optical and X-ray GRB Fundamental Planes as Cosmological Distance Indicators. *Mon. Not. R. Astron. Soc.* **2022**, *514*, 1828–1856. [[CrossRef](#)]
27. Pradyumna, S.; Desai, S. Characterization of the GRB prompt fundamental plane using Fermi-GBM data. *J. High Energy Astrophys.* **2022**, *35*, 77–82. [[CrossRef](#)]
28. Moresco, M.; Amati, L.; Amendola, L.; Birrer, S.; Blakeslee, J.P.; Cantiello, M.; Cimatti, A.; Darling, J.; Valle, M.D.; Fishbach, M.; et al. Unveiling the Universe with Emerging Cosmological Probes. *Living Rev. Relativ.* **2022**, *25*, 6.
29. Bargiacchi, G.; Dainotti, M.G.; Capozziello, S. High-redshift Cosmology by Gamma-Ray Bursts: An overview. *arXiv* **2024**, arXiv:2408.10707.
30. Khadka, N.; Luongo, O.; Muccino, M.; Ratra, B. Do gamma-ray burst measurements provide a useful test of cosmological models? *JCAP* **2021**, *2021*, 042. [[CrossRef](#)]
31. Khadka, N.; Ratra, B. Constraints on cosmological parameters from gamma-ray burst peak photon energy and bolometric fluence measurements and other data. *Mon. Not. R. Astron. Soc.* **2020**, *499*, 391–403. [[CrossRef](#)]
32. Govindaraj, G.; Desai, S. Low redshift calibration of the Amati relation using galaxy clusters. *JCAP* **2022**, *2022*, 069. [[CrossRef](#)]
33. Wang, F.-Y.; Qi, S.; Dai, Z.-G. The updated luminosity correlations of gamma-ray bursts and cosmological implications. *Mon. Not. R. Astron. Soc.* **2011**, *415*, 3423–3433. [[CrossRef](#)]
34. Basilakos, S.; Perivolaropoulos, L. Testing GRBs as Standard Candles. *Mon. Not. R. Astron. Soc.* **2008**, *391*, 411–419. [[CrossRef](#)]
35. Amati, L. The $E_{p,i}$ —Eiso correlation in GRBs: Updated observational status, re-analysis and main implications. *Mon. Not. R. Astron. Soc.* **2006**, *372*, 233–245. [[CrossRef](#)]
36. Yonetoku, D.; Murakami, T.; Nakamura, T.; Yamazaki, R.; Inoue, A.K.; Ioka, K. GRB Formation Rates inferred from the Spectral Peak Energy—Luminosity Relation. *Astrophys. J.* **2004**, *609*, 935. [[CrossRef](#)]
37. Kodama, Y.; Yonetoku, D.; Murakami, T.; Tanabe, S.; Tsutsui, R.; Nakamura, T. Gamma-Ray Bursts in $1.8 < z < 5.6$ Suggest that the Time Variation of the Dark Energy is Small. *Mon. Not. R. Astron. Soc.* **2008**, *391*, L1–L4.
38. Schaefer, B.E. The Hubble Diagram to Redshift >6 from 69 Gamma-Ray Bursts. *Astrophys. J.* **2007**, *660*, 16. [[CrossRef](#)]
39. Scolnic, D.M.; Jones, D.O.; Rest, A.; Pan, Y.C.; Chornock, R.; Foley, R.J.; Huber, M.E.; Kessler, R.; Narayan, G.; Riess, A.G.; et al. The Complete Light-curve Sample of Spectroscopically Confirmed Type Ia Supernovae from Pan-STARRS1 and Cosmological Constraints from The Combined Pantheon Sample. *Astrophys. J.* **2018**, *859*, 101. [[CrossRef](#)]
40. Tang, L.; Li, X.; Lin, H.-N.; Liu, L. Model-independently calibrating the luminosity correlations of gamma-ray bursts using deep learning. *Astrophys. J.* **2021**, *907*, 121. [[CrossRef](#)]
41. Dai, Y.; Zheng, X.-G.; Li, Z.-X.; Gao, H.; Zhu, Z.-H. Redshift evolution of the Amati relation: Calibrated results from the Hubble diagram of quasars at high redshifts. *Astron. Astrophys.* **2021**, *651*, L8. [[CrossRef](#)]
42. Demianski, M.; Piedipalumbo, E.; Sawant, D.; Amati, L. Cosmology with gamma-ray bursts: I. The Hubble diagram through the calibrated $E_{p,i} - E_{iso}$ correlation. *Astron. Astrophys.* **2017**, *598*, A112. [[CrossRef](#)]
43. Demianski, M.; Piedipalumbo, E.; Sawant, D.; Amati, L. Cosmology with gamma-ray bursts: II Cosmography challenges and cosmological scenarios for the accelerated Universe. *Astron. Astrophys.* **2017**, *598*, A113. [[CrossRef](#)]
44. Sari, R.; Piran, T.; Halpern, J.P. Jets in GRBs. *Astrophys. J.* **1999**, *519*, L17. [[CrossRef](#)]
45. Mortlock, D.J.; Warren, S.J.; Venemans, B.P.; Patel, M.; Hewett, P.C.; McMahon, R.G.; Simpson, C.; Theuns, T.; González-Solares, E.A.; Adamson, A.; et al. A luminous quasar at a redshift of $z = 7.085$. *Nature* **2011**, *474*, 616–619. [[CrossRef](#)]
46. Risaliti, G.; Lusso, E. Cosmological constraints from the Hubble diagram of quasars at high redshifts. *Nat. Astron.* **2019**, *3*, 272–277. [[CrossRef](#)]
47. Lusso, E.; Risaliti, G.; Nardini, E.; Bargiacchi, G.; Benetti, M.; Bisogni, S.; Capozziello, S.; Civano, F.; Eggleston, L.; Elvis, M.; et al. Quasars as standard candles III. Validation of a new sample for cosmological studies. *Astron. Astrophys.* **2020**, *642*, A150. [[CrossRef](#)]
48. Khadka, N.; Ratra, B. Determining the range of validity of quasar X-ray and UV flux measurements for constraining cosmological model parameters. *Mon. Not. R. Astron. Soc.* **2021**, *502*, 6140–6156. [[CrossRef](#)]
49. Khadka, N.; Ratra, B. Do quasar X-ray and UV flux measurements provide a useful test of cosmological models? *Mon. Not. R. Astron. Soc.* **2022**, *510*, 2753–2772. [[CrossRef](#)]
50. Khadka, N.; Zajaček, M.; Prince, R.; Panda, S.; Czerny, B.; Martínez-Aldama, M.L.; Jaiswal, V.K.; Ratra, B. Quasar UV/X-ray relation luminosity distances are shorter than reverberation-measured radius-luminosity relation luminosity distances. *Mon. Not. R. Astron. Soc.* **2023**, *522*, 1247–1264. [[CrossRef](#)]
51. Zajaček, M.; Czerny, B.; Khadka, N.; Martínez-Aldama, M.L.; Prince, R.; Panda, S.; Ratra, B. Effect of extinction on quasar luminosity distances determined from UV and X-ray flux measurement. *Astrophys. J.* **2024**, *961*, 229. [[CrossRef](#)]

52. Seikel, M.; Clarkson, C.; Smith, M. Reconstruction of dark energy and expansion dynamics using Gaussian processes. *JCAP* **2012**, *2012*, 036. [[CrossRef](#)]
53. Pedregosa, F.; Varoquaux, G.; Gramfort, A.; Michel, V.; Thirion, B.; Grisel, O.; Blondel, M.; Prettenhofer, P.; Weiss, R.; Dubourg, V.; et al. Scikit-learn: Machine Learning in Python. *J. Mach. Learn. Res.* **2011**, *12*, 2825–2830.
54. D’Agostini, G. Fits, and especially linear fits, with errors on both axes, extra variance of the data points and other complications. *arXiv* **2005**, arXiv:physics/0511182.
55. Foreman-Mackey, D.; Hogg, D.W.; Lang, D.; Goodman, J. emcee: The MCMC Hammer. *Publ. Astron. Soc. Pac.* **2013**, *125*, 306. [[CrossRef](#)]
56. Cao, S.; Zajaček, M.; Panda, S.; Martínez-Aldama, M.L.; Czerny, B.; Ratra, B. Standardizing reverberation-measured C IV time-lag quasars, and using them with standardized Mg II quasars to constrain cosmological parameters. *Mon. Not. R. Astron. Soc.* **2022**, *516*, 1721–1740. [[CrossRef](#)]

Disclaimer/Publisher’s Note: The statements, opinions and data contained in all publications are solely those of the individual author(s) and contributor(s) and not of MDPI and/or the editor(s). MDPI and/or the editor(s) disclaim responsibility for any injury to people or property resulting from any ideas, methods, instructions or products referred to in the content.